

## Geometric multigrid for an implicit-time immersed boundary method

Robert D. Guy · Bobby Philip · Boyce  
E. Griffith

Received: date / Accepted: date

**Abstract** The immersed boundary (IB) method is an approach to fluid-structure interaction that uses Lagrangian variables to describe the deformations and resulting forces of the structure and Eulerian variables to describe the motion and forces of the fluid. Explicit time stepping schemes for the IB method require solvers only for Eulerian equations, for which fast Cartesian grid solution methods are available. Such methods are relatively straightforward to develop and are widely used in practice but often require very small time steps to maintain stability. Implicit-time IB methods permit the stable use of large time steps, but efficient implementations of such methods require significantly more complex solvers that effectively treat both Lagrangian and Eulerian variables simultaneously. Several different approaches to solving the coupled Lagrangian-Eulerian equations have been proposed, but a complete understanding of this problem is still emerging. This paper presents a geometric multigrid method for an implicit-time discretization of the IB equations. This multigrid scheme uses a generalization of box relaxation that is shown to

---

This work was supported in part by University of California Office of The President (UCOP) grant 09-LR-03-116724-GUYR to RG and BP, National Science Foundation (NSF) grant DMS 1160438 to RG, and by American Heart Association grant 10SDG4320049 and NSF grants DMS 1016554 and OCI 1047734 to BG.

---

Robert D. Guy  
Department of Mathematics, University of California, Davis, CA  
Tel.: +1-530-754-9201  
Fax: +1-530-752-6635  
E-mail: guy@math.ucdavis.edu

Bobby Philip  
Oak Ridge National Laboratory, Oak Ridge, TN  
E-mail: philipb@ornl.gov

Boyce E. Griffith  
Leon H. Charney Division of Cardiology, Department of Medicine, New York University School of Medicine, New York, NY  
E-mail: boyce.griffith@nyumc.org

handle problems in which the physical stiffness of the structure is very large. Numerical examples are provided to illustrate the effectiveness and efficiency of the algorithms described herein. These tests show that using multigrid as a preconditioner for a Krylov method yields improvements in both robustness and efficiency as compared to using multigrid as a solver. They also demonstrate that with a time step 100–1000 times larger than that permitted by an explicit IB method, the multigrid-preconditioned implicit IB method is approximately 50–200 times more efficient than the explicit method.

**Keywords** fluid-structure interaction · immersed boundary method · Krylov methods · multigrid solvers · multigrid preconditioners

**Mathematics Subject Classification (2000)** 65F08 · 65M55 · 76M20

## 1 Introduction

The immersed boundary (IB) method [29] was introduced by Peskin [28] to solve problems of fluid-structure interaction in which an elastic structure is immersed in a viscous incompressible fluid. This method was developed to simulate the dynamics of heart valves, but it has subsequently been applied to diverse problems in biofluid dynamics, and it is finding increasing use in other engineering problems [21]. The IB formulation of such problems uses an Eulerian description of the momentum, viscosity, and incompressibility of the fluid-structure system, and it uses a Lagrangian description of the deformation of the immersed structure and forces generated by these deformations. The Eulerian equations are approximated on a Cartesian grid, and the Lagrangian equations are approximated on a curvilinear mesh. Interaction between Eulerian and Lagrangian variables is through integral equations with delta function kernels. When discretized, the IB method uses a regularized version of the delta function to mediate Lagrangian-Eulerian coupling. A key feature of the method is that it does not require conforming discretizations of the fluid and structure; instead, the curvilinear mesh is free to cut through the background Cartesian grid in an arbitrary manner. Consequently, IB simulations do not require dynamic grid generation, even for problems involving very large structural deformations.

Typical implementations of the IB method adopt a fractional step approach to time stepping. In the simplest version of such a scheme, the Eulerian velocity and pressure fields are updated for a fixed configuration of the immersed structure, and then the position of the Lagrangian structure is updated from the newly computed velocity field. This approach effectively decouples the Eulerian and Lagrangian equations, and solvers are needed only for the Eulerian equations (i.e., the incompressible Stokes or Navier-Stokes equations), for which fast Cartesian grid solution methods are available. However, because this fractional step approach yields an explicit time stepping method for the structural dynamics problem, maintaining stability requires time steps that are small enough to resolve all of the elastic modes of the discrete equations.

In many applications, these elastic time scales are well below the physical time scales of interest. Even for relatively simple elasticity models, the largest stable time step size scales like  $\Delta t = O(\Delta s^2)$ , in which  $\Delta s$  is the Lagrangian mesh spacing. For problems involving bending-resistant elastic elements, the largest stable time step scales like  $\Delta t = O(\Delta s^4)$ . Consequently, high-resolution IB simulations can require extremely large numbers of time steps, making it challenging to perform simulations over long time scales.

Much effort has been devoted both to understanding and to alleviating the severe time step restriction of fractional step IB methods [31,23,8]. One approach is to develop implicit or semi-implicit time stepping schemes that allow for time steps that do not resolve all of the elastic modes of the discrete system; however, despite decades of work, such schemes are still not widely used in practice. The solution methods used in early implicit IB methods were not efficient and were not competitive with explicit methods [36], and some semi-implicit methods intended to allow for large time steps still suffered from significant time step restrictions [20,18]. Newren et al. [23] analyzed the origin of instability in semi-implicit IB methods using energy arguments, and they gave sufficient conditions to achieve unconditionally stability in the sense that the total energy is bounded independent of time step size. An important result by Newren et al. [23] is that it is not necessary to employ a *fully* implicit time discretization to achieve unconditional stability, but the stable time stepping schemes proposed therein do simultaneously solve for both the Eulerian velocity field and the Lagrangian structural configuration. However, as indicated by the early experience with implicit IB methods developing efficient solvers for the coupled equations is challenging.

More recently, a number of stable semi-implicit [24,14,15,5] and fully implicit [22,17] IB methods have been developed. The efficiency of these methods is generally competitive with explicit methods, and in some special cases, these implicit schemes can be faster than explicit methods by several orders of magnitude. Many implicit methods use a Schur complement approach to reduce the coupled Lagrangian-Eulerian equations to purely Lagrangian equations [22,5,4]. These methods achieve a substantial speed-up over explicit methods when there are relatively few Lagrangian mesh nodes [5]. In addition, some methods require that the boundaries be smooth, closed curves [14,15]. An open question is whether there exist robust, general-purpose implicit methods that are more efficient than explicit methods, or whether specialized methods must be developed for specific problems.

Newren et al. [24] explored the use of unpreconditioned Krylov methods for solving the linearized IB equations in the context of different test problems. They found that the relative efficiency of the implicit methods depended on the problem, and unpreconditioned Krylov methods were generally at least comparable in speed to explicit methods. These results suggest that with appropriate preconditioning, this approach will offer a significant improvement over explicit methods. One way to achieve generally applicable and robust implicit methods is through the development of robust preconditioners for the linearized equations. This is the approach we take in this paper.

In previous work [13], we developed a multigrid method for a model problem related to implicit time discretizations of the IB equations. This model problem ignored the inertial terms and the incompressibility constraint. The multigrid solver introduced in this earlier work was more efficient than explicit-time methods for the model problem, but the increase in efficiency was not large for the very stiff problems for which implicit time stepping methods are most clearly needed. When used as a preconditioner for a Krylov solver, however, the method was very efficient, even for very stiff problems.

In this paper, we extend the methods developed for the model IB equations [13] to problems of incompressible flow. Specifically, we consider a version of the IB method for the steady incompressible Stokes equations. (The extension of the method to the unsteady Stokes equations, or to the full Navier-Stokes equations, is straightforward but is not considered here.) Unlike most other work on developing efficient solvers for implicit IB methods, here we focus on a formulation of the problem in which we effectively eliminate the *structural* degrees of freedom by a Schur complement approach. The system that we solve is therefore defined only on the background Cartesian grid. As in earlier work [13], we take advantage of the structure of the Cartesian grid to develop geometric multigrid methods for the linear systems of our implicit-time discretization. The key contributions of this paper are the development of generalized box-relaxation (also known as Vanka) smoothers for this formulation of the IB equations, and the extension of these box-relaxation smoothers to larger collections of grid cells, as needed to obtain good performance for problems in which the elastic structure is extremely stiff. We perform numerical tests that demonstrate the performance of these algorithms, and we show that with these solvers, the implicit scheme has the potential to be significantly more efficient than a similar explicit IB method.

## 2 Immersed Boundary Equations

### 2.1 Continuum equations

Let  $\boldsymbol{x} \in \Omega$  denote fixed physical coordinates, with  $\Omega \subset \mathbb{R}^2$  denoting the physical domain. Let  $\boldsymbol{s} \in \Gamma$  denote material coordinates attached to the immersed structure, with  $\Gamma \subset \mathbb{R}^2$  denoting the Lagrangian coordinate domain.<sup>1</sup> The physical location of material point  $\boldsymbol{s}$  at time  $t$  is given by  $\boldsymbol{X}(\boldsymbol{s}, t) \in \Omega$ . (In general, we use lowercase letters for quantities expressed in Eulerian coordinates and uppercase letters for quantities expressed in Lagrangian coordinates.) In the absence of other loading, the forces generated by the deformations of the

---

<sup>1</sup> We remark that the name *immersed boundary method* suggests that the elastic structure is a thin interface (i.e., an object of codimension one with respect to the fluid). While this is the case in many applications of the IB method, this formulation applies equally well to immersed structures that have nonzero thickness. We restrict our tests to two spatial dimensions and to structures of nonzero thickness. The extension to three spatial dimensions is straightforward, and in the concluding discussion, we comment on the differences between thick and thin structures.

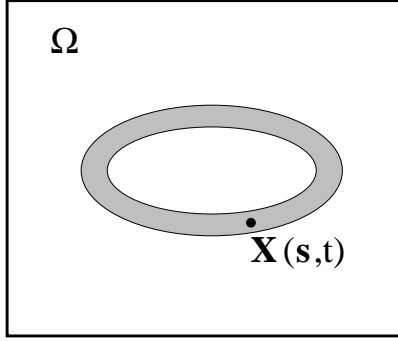


**Fig. 1** The physical domain  $\Omega$  contains the immersed elastic structure. The position of each material point  $\mathbf{s}$  at time  $t$  is given by  $\mathbf{X}(\mathbf{s}, t) \in \Omega$ .

structure drive the motion of the fluid. We assume that the immersed structure is neutrally buoyant, so that all of the boundary force is transmitted to the fluid. The equations we consider in this paper are

$$\Delta \mathbf{u}(\mathbf{x}, t) - \nabla p(\mathbf{x}, t) + \mathbf{f}(\mathbf{x}, t) = 0, \quad (1)$$

$$\nabla \cdot \mathbf{u}(\mathbf{x}, t) = 0, \quad (2)$$

$$\mathbf{f}(\mathbf{x}, t) = \int_{\Gamma} \mathbf{F}(\mathbf{s}, t) \delta(\mathbf{x} - \mathbf{X}(\mathbf{s}, t)) \, d\mathbf{s}, \quad (3)$$

$$\frac{\partial \mathbf{X}(\mathbf{s}, t)}{\partial t} = \mathbf{U}(\mathbf{s}, t) = \int_{\Omega} \mathbf{u}(\mathbf{x}, t) \delta(\mathbf{x} - \mathbf{X}(\mathbf{s}, t)) \, d\mathbf{x}, \quad (4)$$

in which  $\mathbf{u}(\mathbf{x}, t) = (u(\mathbf{x}, t), v(\mathbf{x}, t))$  is the velocity field of the fluid-structure system,  $p(\mathbf{x}, t)$  is the pressure,  $\mathbf{f}(\mathbf{x}, t)$  is the Eulerian elastic force density generated by the immersed structure, and  $\mathbf{F}(\mathbf{s}, t)$  is the Lagrangian elastic force density generated by the immersed structure. The first two equations are the incompressible Stokes equations, which here describe the motion of a fluid-structure system in which the influence of inertia is negligible. The last two equations describe the coupling between the Eulerian and Lagrangian frames. The integral operator in (3) that determines the Eulerian force density from the Lagrangian force density is called the *spreading* operator, which we denote by  $S[\mathbf{X}]$ . The *interpolation* operator that transfers the velocity to the structure is the adjoint of the spreading operator. Using this notation, equations (3) and (4) can be compactly expressed as  $\mathbf{f} = S[\mathbf{X}] \mathbf{F}$  and  $\partial \mathbf{X} / \partial t = \mathbf{U} = S[\mathbf{X}]^* \mathbf{u}$ , respectively.

A constitutive law for the immersed elastic material is needed to complete the description of the system. Herein, we consider structures that consist of a collection of linear elastic fibers under tension. We choose the Lagrangian coordinate system so that for  $\mathbf{s} = (s_1, s_2)$ ,  $s_1$  is a parametric coordinate along each fiber, and  $s_2$  is constant on each fiber. Let  $\boldsymbol{\tau}$  be the unit vector tangent to the fiber direction, which is given by  $\boldsymbol{\tau} = \partial \mathbf{X} / \partial s_1 / \|\partial \mathbf{X} / \partial s_1\|$ . The tension in each fiber is taken to be  $T = \gamma \|\partial \mathbf{X} / \partial s_1\|$ , in which  $\gamma$  is a constant that

characterizes the elastic stiffness of the fiber. Under these assumptions, the Lagrangian force density is

$$\mathbf{F}(\mathbf{s}, t) = \frac{\partial}{\partial s_1} (T\boldsymbol{\tau}) = \gamma \frac{\partial^2 \mathbf{X}}{\partial s_1^2}. \quad (5)$$

This constitutive law corresponds to an elastic shell that is composed of a continuum of circumferential elastic fibers [1,11,12]. It is also equivalent to a version of an incompressible neo-Hookean elastic material. Note that in this formulation, the overall structural response is actually viscoelastic, because the structural stress tensor includes a viscous term that is identical to that of the fluid. Immersed boundary methods have been developed which include a separate structure viscosity [7,16,32]. We take the structure viscosity to be equal to the fluid viscosity here for simplicity; however, as discussed in Section 8, this is not a fundamental limitation of our method.

## 2.2 Spatial discretization

The physical domain  $\Omega$  is taken to be rectangular and in our computations is discretized by a uniform Cartesian grid with square cells of width  $\Delta x = \Delta y = h$ . We use a staggered-grid discretization of the incompressible Stokes equations in which the components of the velocity and Eulerian body force are approximated at the centers of the cell edges to which that component is normal, and in which the pressure is approximated at the cell centers; see Figure 2. The Laplacian, gradient, and divergence operators are discretized using standard second-order finite differences, and the corresponding discrete operators are denoted by  $\Delta_h$ ,  $\nabla_h \cdot$ , and  $\nabla_h$ , respectively.

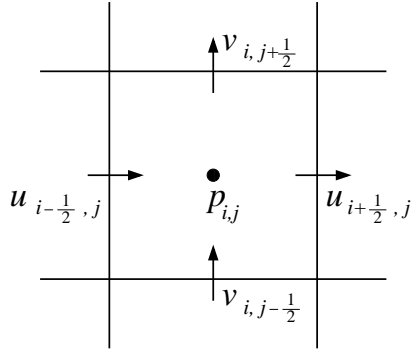


**Fig. 2** Staggered grid discretization in which the velocity field  $\mathbf{u} = (u, v)$  and Eulerian body force  $\mathbf{f} = (f_1, f_2)$  are approximated at the centers of the cell edges, and in which the pressure  $p$  is approximated at the cell centers.

The immersed structure is discretized using a fiber-aligned mesh with nodes that are equally spaced in the Lagrangian coordinate system with spacing

$\Delta s_1 = \Delta s_2 = \Delta s$  is each direction. The physical location of Lagrangian node  $\mathbf{s}_{k,l}$  is denoted by  $\mathbf{X}_{k,l}$ . The second derivative operator that appears in the boundary force (5) is discretized using standard three-point centered differencing. The Lagrangian elastic force density at node  $\mathbf{s}_{k,l}$  is

$$\mathbf{F}_{k,l} = \gamma \frac{\mathbf{X}_{k-1,l} - 2\mathbf{X}_{k,l} + \mathbf{X}_{k+1,l}}{\Delta s^2} = \gamma (A_f \mathbf{X})_{k,l}, \quad (6)$$

in which we use  $A_f$  to denote the discrete force-generation operator.

To approximate the Lagrangian-Eulerian interaction equations, we use a two-dimensional regularized delta function  $\delta_h(\mathbf{x})$  that is the tensor product of two one-dimensional regularized delta functions,  $\delta_h^1(r)$ , so that for  $\mathbf{x} = (x, y)$  and  $\mathbf{X} = (X, Y)$ ,

$$\delta_h(\mathbf{x} - \mathbf{X}) = \delta_h^1(x - X) \delta_h^1(y - Y). \quad (7)$$

In this work, we use

$$\delta_h^1(r) = \begin{cases} \frac{1}{4h} (1 + \cos(\frac{\pi r}{2})) & \text{if } r < 2h, \\ 0 & \text{otherwise.} \end{cases} \quad (8)$$

The discretized spreading operator  $S_h[\mathbf{X}]$  is defined for  $\mathbf{f} = (f_1, f_2)$  and for  $\mathbf{F} = (F_1, F_2)$  by

$$(f_1)_{i-1/2,j} = \sum_{k,l} (F_1)_{k,l} \delta_h(\mathbf{x}_{i-1/2,j} - \mathbf{X}_{k,l}) \Delta s^2, \quad (9)$$

$$(f_2)_{i,j-1/2} = \sum_{k,l} (F_2)_{k,l} \delta_h(\mathbf{x}_{i,j-1/2} - \mathbf{X}_{k,l}) \Delta s^2, \quad (10)$$

in which  $\mathbf{x}_{i-1/2,j}$  and  $\mathbf{x}_{i,j-1/2}$  denote the positions of the centers of the edges of the grid cells, where the velocity and force components are approximated. Similarly, the discrete interpolation operator, which is the adjoint of the discrete spreading operator, is defined by

$$\left( \frac{\partial X}{\partial t} \right)_{k,l} = U_{k,l} = \sum_{i,j} u_{i-1/2,j} \delta_h(\mathbf{x}_{i-1/2,j} - \mathbf{X}_{k,l}) h^2, \quad (11)$$

$$\left( \frac{\partial Y}{\partial t} \right)_{k,l} = V_{k,l} = \sum_{i,j} v_{i,j-1/2} \delta_h(\mathbf{x}_{i,j-1/2} - \mathbf{X}_{k,l}) h^2. \quad (12)$$

## 2.3 Temporal discretizations

### 2.3.1 Explicit-time method

Typical implementations of the IB method use a fractional time stepping approach to solve the equations of motion. In the simplest version of such a scheme, the fluid velocity and pressure are updated while keeping the position

of the structure fixed, and then the structural position is updated using the newly computed velocity. We refer to this method as the explicit-time method. For the model equations considered herein, the explicit-time method advances the solution variables from time  $t^n = n\Delta t$  to time  $t^{n+1} = (n+1)\Delta t$  via

$$\Delta_h \mathbf{u}^{n+1} - \nabla_h p^{n+1} + S_h^n \mathbf{F}^n = 0, \quad (13)$$

$$\nabla_h \cdot \mathbf{u}^{n+1} = 0, \quad (14)$$

$$\mathbf{F}^n = \gamma A_f \mathbf{X}^n \quad (15)$$

$$\mathbf{X}^{n+1} = \mathbf{X}^n + \Delta t (S_h^n)^* \mathbf{u}^{n+1}, \quad (16)$$

in which  $S_h^n = S_h[\mathbf{X}^n]$ . Notice that the explicit-time method requires the solution of only the incompressible Stokes system.

### 2.3.2 Implicit-time method

The implicit-time method is similar to the explicit-time method, except that we now use backward Euler to update the structural position, and we now compute the structural forces using the newly computed positions. The implicit method advances the solution variables via

$$\Delta_h \mathbf{u}^{n+1} - \nabla_h p^{n+1} + S_h^n \mathbf{F}^{n+1} = 0, \quad (17)$$

$$\nabla_h \cdot \mathbf{u}^{n+1} = 0, \quad (18)$$

$$\mathbf{F}^{n+1} = \gamma A_f \mathbf{X}^{n+1}, \quad (19)$$

$$\mathbf{X}^{n+1} = \mathbf{X}^n + \Delta t (S_h^n)^* \mathbf{u}^{n+1}. \quad (20)$$

Notice that in this time stepping scheme, the structural positions used to define the spreading and interpolation operators are lagged in time. As shown by Newren et al. [23], this scheme is unconditionally stable, despite the fact that the positions of the spreading and interpolation operators are treated explicitly rather than implicitly. This is quite fortuitous; if it were necessary to treat the spreading and interpolation operators implicitly, then we would be faced with a *nonlinear* system of equations.

We use (19) and (20) to eliminate the unknown force  $\mathbf{F}^{n+1}$  from (17) to yield a system in which the only unknowns are the velocity  $\mathbf{u}^{n+1}$  and pressure  $p^{n+1}$ ,

$$(\Delta_h + \alpha S_h^n A_f (S_h^n)^*) \mathbf{u}^{n+1} - \nabla_h p + S_h^n A_f \mathbf{X}^n = 0 \quad (21)$$

$$\nabla_h \cdot \mathbf{u}^{n+1} = 0, \quad (22)$$

with  $\alpha = \Delta t \gamma$ .

To advance the full system in time, we first solve equations (21)–(22) for the velocity and pressure, and we then use equation (20) to update the position of the structure. The advantages of reducing the full system (17)–(20) to (21)–(22) are that the only unknowns in (21)–(22) are the Eulerian velocity and pressure, and that the equations are defined on a structured grid. The elimination of the Lagrangian unknowns facilitates the development of geometric multigrid methods for the IB equations.

### 3 Multigrid

We provide a brief sketch of geometric multigrid methods, focusing on details specific to our application. For a detailed description, the reader is referred to Refs. [35, 3].

Let  $\Omega_h$  represent the discretized physical domain with Cartesian grid spacing  $h$ . The linear system (21)–(22) on  $\Omega_h$  can be written as

$$\begin{bmatrix} (\Delta_h + \alpha S_h A_f S_h^*) - \nabla_h & \\ \nabla_h \cdot & 0 \end{bmatrix} \begin{bmatrix} \mathbf{u}^{n+1} \\ p^{n+1} \end{bmatrix} = \begin{bmatrix} -S_h A_f \mathbf{X}^n \\ 0 \end{bmatrix}, \quad (23)$$

which we denote by

$$\mathcal{A}_h \mathbf{w}_h = \mathbf{b}_h. \quad (24)$$

To simplify the notation, we set  $S_h \equiv S_h^n$  and  $S_h^* \equiv (S_h^n)^*$ . Notice, however, that  $S_h$  and  $S_h^*$  are generally time-dependent discrete operators, as is  $\mathcal{A}_h$ .

Let  $I_{2h \leftarrow h}$  denote the operator that *restricts* solution data to  $\Omega_{2h}$  from  $\Omega_h$ , let  $I_{h \leftarrow 2h}$  denote the operator that *prolongs* solution data to  $\Omega_h$  from  $\Omega_{2h}$ , and let  $\mathcal{A}_{2h}$  denote the coarse-grid operator defined on  $\Omega_{2h}$ . (Definitions for each of these operators are provided below.) The smoothers used in this work, which are a key aspect of the overall solution algorithm, are specified below in the context of specific numerical examples. We specifically consider a generalization of a standard box-relaxation smoother in Section 5, and an extension of this approach to “big” boxes in Sections 6 and 7. A geometric multigrid V-cycle for (24) is given by Algorithm 1.

**Algorithm 1:**  $\mathbf{w}_h \leftarrow MG(\mathbf{w}_h, \mathbf{b}_h, \Omega_h, \nu_1, \nu_2)$

- (1) **if**  $\Omega_h$  is the coarsest level
- (2)     Solve the coarse-grid equation:  $\mathbf{w}_h \leftarrow (\mathcal{A}_h)^{-1} \mathbf{b}_h$
- (3) **else**
- (4)     Perform  $\nu_1$  *presmoothing* sweeps for  $\mathcal{A}_h \mathbf{w}_h = \mathbf{b}_h$  on  $\Omega_h$  using initial guess  $\mathbf{w}_h$
- (5)     Compute the residual on  $\Omega_h$  and restrict it from  $\Omega_h$  to  $\Omega_{2h}$ :  $\mathbf{r}_{2h} \leftarrow I_{2h \leftarrow h} (\mathbf{b}_h - \mathcal{A}_h \mathbf{w}_h)$
- (6)     Compute an approximate solution to the error equation  $\mathcal{A}_h \mathbf{e}_h = \mathbf{r}_h$  on  $\Omega_{2h}$ :  $\mathbf{e}_{2h} \leftarrow MG(\mathbf{0}, \mathbf{r}_{2h}, \Omega_{2h}, \nu_1, \nu_2)$
- (7)     Prolong the coarse-grid correction from  $\Omega_{2h}$  to  $\Omega_h$  and update the solution on  $\Omega_h$ :  $\mathbf{w}_h \leftarrow \mathbf{w}_h + I_{h \leftarrow 2h} \mathbf{e}_{2h}$
- (8)     Perform  $\nu_2$  *postsmoothing* sweeps for  $\mathcal{A}_h \mathbf{w}_h = \mathbf{b}_h$  on  $\Omega_h$  using initial guess  $\mathbf{w}_h$

Multigrid methods are intended to work on all components of the error in a given approximation to the solution of (24) by a combination of fine-grid relaxation (steps 4 and 8 in Algorithm 1) and coarse-grid correction (steps 5–7 in Algorithm 1). In well-designed multigrid methods, fine-grid relaxation and coarse-grid correction are complementary processes: the errors that are not damped by the fine-grid relaxation are damped by the coarse-grid correction, and vice versa. If these processes are not complementary (i.e., do not damp all error modes), then the method will yield poor convergence rates; if these

processes overlap (i.e., damp the same components of the error), then the method will provide sub-optimal efficiency.

### 3.1 Grid transfer operators: Restriction and prolongation

We use standard geometric coarsening of the Cartesian grid in which a hierarchy of successively coarser grids  $\Omega_h, \Omega_{2h}, \Omega_{4h}, \dots$  is generated. Because approximations to the components of the velocity and the pressure are all defined at different spatial locations, different operators are required to transfer these values between levels of the hierarchy of discretizations.

For the pressure, we obtain coarse cell-centered values by averaging the four overlying fine cell-centered values. The stencil and coefficients of the pressure restriction operator are given by

$$R_p = \frac{1}{4} \begin{bmatrix} 1 & 1 \\ * & \\ 1 & 1 \end{bmatrix}, \quad (25)$$

in which “\*” denotes the position of the coarse value. To prolong pressure data from coarser grids to finer grids, we use constant prolongation, so that for each coarse grid cell, each overlying fine grid cell takes the underlying coarse grid value.

Restriction of the  $x$ -components of the velocity ( $u$ ) is done by two-point averaging in the  $y$ -direction and full-weighting in the  $x$ -direction. The stencil and coefficients for the operator are

$$R_u = \frac{1}{8} \begin{bmatrix} 1 & 2 & 1 \\ * & & \\ 1 & 2 & 1 \end{bmatrix}. \quad (26)$$

A similar procedure, but with two-point averaging in the  $x$ -direction and full-weighting in the  $y$ -direction, is used to restrict the  $y$  components of the velocity ( $v$ ). In each case, standard bilinear interpolation is used to prolong components of the velocity from coarser grids to finer grids.

We remark that these transfer operators are the standard ones for staggered-grid discretizations of incompressible flow problems [35], but other transfer operators could be used. See Niestegge et al. [25] for a study of the performance of several different combinations of interpolation and restriction operators for the Stokes equations. We experimented with different combinations of operators, and we found these standard operators gave the best overall efficiency.

### 3.2 Coarse-grid operator

Coarse-grid correction requires the formation of a coarse-grid operator for each of the coarser levels of the grid hierarchy. In geometric multigrid, the two most common approaches are direct re-discretization of the PDE on each

grid level, and algebraic construction via a Galerkin procedure. In previous work on a model of the IB method, we found that Galerkin coarsening was necessary for convergence [13]. However, Galerkin coarsening of the Stokes equations is expensive because the Galerkin coarse-grid operators have large stencils. Because re-discretization works well for the Stokes equations alone (i.e., without the IB elasticity operator  $S_h A_f S_h^*$ ), we employ a hybrid approach: We re-discretize the Stokes equations, and we use Galerkin coarsening for the Eulerian elasticity operator  $S_h A_f S_h^*$ . Specifically, the coarse-grid operator is

$$\mathcal{A}_{2h} = \begin{bmatrix} (\Delta_{2h} + \alpha I_{2h \leftarrow h} S_h A_f S_h^* I_{h \leftarrow 2h}) & -\nabla_{2h} \\ \nabla_{2h} & 0 \end{bmatrix}. \quad (27)$$

Coarser versions of  $S_h A_f S_h^*$ , e.g., on  $\Omega_{4h}, \Omega_{8h}, \dots$ , are constructed recursively.

### 3.3 Multigrid preconditioning

As we have remarked, multigrid is a highly effective solver when smoothing and coarse-grid correction work in a complementary manner to eliminate all error modes, and with the smoothers used in this work, the present algorithm achieves high efficiency for the Stokes problem. As the stiffness of the immersed boundary increases in the implicit-time method, however, the discrete operator becomes increasingly less ‘‘Stokes-like’’ in the vicinity of the immersed structure, and the performance of the multigrid algorithm suffers.

In our previous work on applying multigrid to a model of the IB method [13], we found that multigrid alone was a poor solver for large stiffnesses but that it performed very effectively as a preconditioner for Krylov methods. We follow the same approach here, and in our numerical experiments, we explore the performance of multigrid as both a solver and as a (right) preconditioner for GMRES [30]. For more details on the general use of multigrid preconditioned Krylov methods, see Refs. [34, 27], and see Refs. [33, 39, 6] for specific examples from fluid mechanics.

## 4 Test Problem Description

We explore the performance of the multigrid method as a solver and as a preconditioner for a range of elastic stiffnesses of the immersed structure. Except where otherwise noted, the physical domain  $\Omega$  is the unit square  $[0, 1]^2$ , and Dirichlet conditions are imposed on the velocity along  $\partial\Omega$  to yield lid-driven-cavity flow. Specifically, all components of the velocity are set to zero on the boundary except on the top wall, where the tangential velocity is  $u(x, 1) = (1 - \cos(2\pi x))/2$ .

In all cases, the immersed structure is the annulus with initial positions

$$\mathbf{X}(s_1, s_2) = \left( x_c + (r + s_2) \cos(s_1/r), y_c + (r + s_2) \sin(s_1/r) \right), \quad (28)$$

in which  $\mathbf{x}_c = (x_c, y_c) = (0.5, 0.5)$  is the center of the annulus, which also generally corresponds to the center of  $\Omega$  in our tests, and in which  $r = 1/4$  is the inner radius of the annulus. The Lagrangian coordinate domain is  $(s_1, s_2) \in [0, 2\pi r) \times [0, w]$ , with  $w = 1/16$  indicating the thickness of the annulus. This domain is discretized using a regular grid with  $M_1$  points in the  $s_1$  direction and  $M_2$  points in the  $s_2$  direction. We choose  $M_1 = 19N/8$  and  $M_2 = 3N/32 + 1$ , in which  $N$  is the number of grid cells used to discretize one direction in the Eulerian domain, so that  $h = 1/N$ . We restrict  $N$  to be a power of two, so that  $M_1$  and  $M_2$  are integers. The physical distance between adjacent Lagrangian nodes is approximately  $2/3$  of the Eulerian grid spacing  $h$ .

A similar thick ring structure has been used in other immersed boundary benchmarking tests on accuracy [12], volume conservation [10], and implicit time stepping [22]. A notable difference between our test and past tests is that we drive a background flow through the boundary condition so that the physical time scale is set by the background flow, not by the stiffness of the structure. For large elastic stiffness, the elastic time scale is well below the physical flow time scale, which is a characteristic of problems that benefit most from efficient implicit-time methods.

#### 4.1 Characterizing the elastic stiffness

The explicit-time method given by equations (13)–(16) is equivalent to the forward Euler scheme applied to

$$\frac{\partial \mathbf{X}}{\partial t} = \gamma S_h^* \mathcal{L}_h^{-1} S_h A_f \mathbf{X}, \quad (29)$$

in which  $\mathcal{L}_h^{-1}$  is the operator that maps fluid forces to the fluid velocity by solving the Stokes system, and  $\gamma$  is the stiffness of the elastic structure (see (5)). The stability of this scheme is determined by the single parameter

$$\alpha = \gamma \Delta t. \quad (30)$$

The forward Euler method applied to (29) is stable provided

$$|1 + \alpha \lambda| \leq 1, \quad (31)$$

for all  $\lambda$  which are eigenvalues of  $S_h^* \mathcal{L}_h^{-1} S_h A_f$ . Because  $S_h^* \mathcal{L}_h^{-1} S_h$  is symmetric and positive semidefinite and  $A_f$  is symmetric and negative semidefinite, the eigenvalues of their product are all real and nonpositive. Therefore the stability condition (31) is equivalent to the condition

$$\alpha \rho \leq 2, \quad (32)$$

where  $\rho$  is the spectral radius of the matrix  $S_h^* \mathcal{L}_h^{-1} S_h A_f$ . Let  $\alpha_{\text{exp}}$  denote the maximum value of  $\alpha$  for which the explicit-time method is stable, which is defined by

$$\alpha_{\text{exp}} = \frac{2}{\rho}, \quad (33)$$

In Table 1, we report values of  $\alpha_{\text{exp}}$  for different grid spacings.

**Table 1**  $\alpha_{\text{exp}}$  is the maximum value of the stiffness  $\alpha = \gamma\Delta t$  for which the explicit-time scheme is stable for grid spacing  $h$ .

$h$	$2^{-5}$	$2^{-6}$	$2^{-7}$	$2^{-8}$
$\alpha_{\text{exp}}$	6.09	3.93	2.82	2.28

## 5 Box Relaxation

Several different smoothers for the Stokes equations have been developed. Two large classes of smoothers are distributive smoothers [2] and collective smoothers [37]. Distributive relaxation techniques, originally pioneered by Brandt and Dinar [2], involve a transformation of the equations so that the individual velocity components and pressure are smoothed separately [2, 19, 38]. Collective or box relaxation, originally proposed by Vanka [37], involves smoothing the velocity and the pressure simultaneously. Oosterlee and Washio [26] provide a comparison of distributed and collective smoothers for incompressible flow problems.

Distributed smoothers for the Stokes equations are straightforward to implement because they involve smoothing only scalar problems; however, extending distributive smoothers to the implicit IB equations is challenging. In particular, it is not clear whether it is possible to transform the saddle point problem (23) into a form that permits the decoupled smoothing of the velocity and pressure. In this work, we instead employ box relaxation. Box relaxation is essentially a generalization of point smoothers like Jacobi or Gauss-Seidel to multi-component systems, including saddle-point systems. The basic idea of box relaxation is to sweep over the grid cells and, in each cell, to solve locally the discrete equations restricted to that cell. In the present context, a 5-by-5 system of equations must be solved for each cell that involves the four velocity components and the one pressure. We order the boxes lexicographically, and we update the unknowns box-by-box in a block Gauss-Seidel-like manner.

### 5.1 Solver performance

As an initial test of the performance of the multigrid method as a solver and as a preconditioner, we consider an Eulerian grid with  $h = 2^{-5}$  and the corresponding Lagrangian mesh, we set the initial guess for the velocity and pressure to zero, and we compute the number of iterations needed to reduce the residual by a factor of  $10^{-6}$ . We use V-cycles with one pre-smoothing sweep and one post-smoothing sweep ( $\nu_1 = \nu_2 = 1$ ). Figure 3 shows the resulting iteration counts as a function of  $\alpha/\alpha_{\text{exp}}$  for both multigrid as a solver and as a preconditioner for GMRES. The ratio  $\alpha/\alpha_{\text{exp}}$  may be interpreted as follows. For a given elastic stiffness,  $\alpha/\alpha_{\text{exp}}$  represents the size of the time step relative to the maximum allowed by the explicit-time method. We call this ratio the *relative stiffness*.

The iteration count of the multigrid method is essentially constant (9 iterations) up to a relative stiffness of about 10, at which point the iteration count

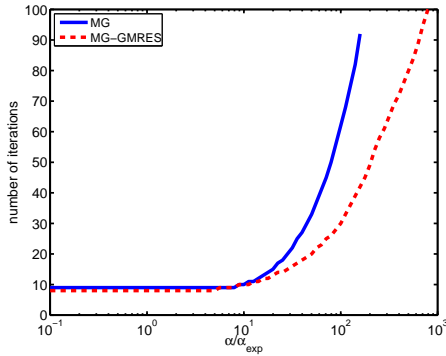


**Fig. 3** Iteration counts for the multigrid solver and for multigrid-preconditioned GMRES to reduce the residual by a factor of  $10^{-6}$  as a function of the stiffness. The stiffness is scaled by the maximum stiffness from the explicit-time scheme,  $\alpha_{\text{exp}}$ .

begins to increase rapidly. For  $\alpha/\alpha_{\text{exp}} = 100$ , the multigrid solver takes 62 iterations to converge, and the multigrid solver fails to converge for a relative stiffness of  $\alpha/\alpha_{\text{exp}} \approx 160$ .

The iteration count for the MG-GMRES method is also essentially constant (8 iterations) up to a relative stiffness of 10. After this point, the iteration count begins to increase, but not as rapidly as when we use multigrid as a solver. For  $\alpha/\alpha_{\text{exp}} = 100$ , the iteration count is 30, or about half that of multigrid alone. Unlike the stand-alone multigrid solver, MG-GMRES does not appear ever to diverge, but we stopped after 100 iterations. This maximum number of iterations was reached at a relative stiffness of  $\alpha/\alpha_{\text{exp}} \approx 800$ .

If we assume that a V-cycle for the Stokes-IB system takes about the same amount of work as a V-cycle applied to the Stokes equations (i.e., without the IB elasticity operator), then we can use the iteration counts to estimate the efficiency of this approach.<sup>2</sup> For  $\alpha/\alpha_{\text{exp}} = 100$ , the multigrid algorithm takes 62 iterations. To reach the same point in time, an explicit method would require at least 100 time steps and require 9 iterations per time step. Therefore we estimate the implicit method would be  $100 \cdot 9/62 \approx 14.5$  times more efficient. A similar estimate for MG-GMRES suggests that the implicit method would be about 27 times more efficient at this value of stiffness. These are likely overestimates of the efficiency gain, and we will return to more careful efficiency comparisons for a time-dependent problem in Section 7.

For very stiff problems MG-GMRES is more efficient than the stand-alone multigrid solver. For nonstiff problems (e.g.,  $\alpha/\alpha_{\text{exp}} < 10$ ), stand-alone multigrid is more efficient because one iteration of MG-GMRES is more expensive than one iteration of multigrid. However, MG-GMRES is the more robust solver; it does not fail to converge as the stiffness increases.

<sup>2</sup> In practice, the extent to which this assumption holds depends on the relative densities of the Eulerian and Lagrangian discretizations.

## 5.2 Spectrum of the multigrid operator

To explore the relatively poor performance and ultimate failure of the stand-alone multigrid solver at large stiffness, we explicitly construct the multigrid iteration matrix and compute its eigenvalues. We construct the multigrid iteration matrix using the procedure outlined in Ref. [35]. The idea is as follows: Let the values of the velocity and pressure be organized into a single vector  $\mathbf{w} = [u; v; p]$ . To generate the  $k^{\text{th}}$  column of the multigrid matrix, we set  $\mathbf{w}_j = \delta_{jk}$ , in which  $\delta_{jk}$  is the Kronecker delta, and we perform one multigrid cycle.

In Figure 4, we plot the eigenvalues of the multigrid iteration matrix in the complex plane for four different relative stiffness. We also report the spectral radius  $\rho$  of the operator on the space in which the mean pressure is set to zero. Because the pressure is unique only up to additive constants, there is always an eigenvalue of 1 that corresponds to pressure fields that are constant on  $\Omega_h$ . This trivial eigenspace does not affect the convergence of the method.

The eigenvalues of the iteration matrix for the Stokes problem (i.e., with  $\alpha = 0$ ) are shown in Figure 4(a). All of the nontrivial eigenvalues are clustered within a disc of radius 0.24 around the origin. The spectrum is very similar at relative stiffness 1. In fact, the spectral radius is slightly smaller than in the Stokes case. At relative stiffness 10, most of the eigenvalues are again clustered around the origin, but we now see a small number of that are away from the origin. The spectral radius is 0.30, which indicates a slight increase in the number of iterations over the Stokes system ( $\alpha = 0$ ). We remark that we did not observe an increase in the iteration count in our computational experiment until the relative stiffness increased above 10.

At relative stiffness 100, the spectral radius is 0.85, which is consistent with our observation of slow convergence. There are now a notable number of “large” eigenvalues, but the majority of them are still clustered near the origin. For example, only about 5% of the eigenvalues are outside the disc of radius 0.25, and only 1.5% are outside the disc of radius 0.5. This eigenvalue distribution explains why multigrid is a poor solver but an effective preconditioner. It is effectively damping a large eigenspace but poorly damping a small eigenspace. When used as a preconditioner for stiff problems, multigrid acts to cluster most of the eigenvalues around 1, and it leaves a small set of scattered eigenspaces which are approximated by a small Krylov space. For a detailed analysis of this situation, see Ref. [27]. Additionally, we note the similarity to multiphase flow applications with sharp variation in material properties. In these applications, it has been observed that multigrid is a poor solver but a very effective preconditioner for Krylov methods [39,33].

We examine the velocity and pressure that correspond to the slowly converging modes at large stiffness to attempt to obtain insight into the poor performance of multigrid. In Figure 5, we plot the two components of the velocity and pressure as functions of space for the mode with eigenvalue  $\approx 0.85$ . We see that this mode exhibits high-frequency spatial oscillations, and that the oscillations are concentrated near the immersed structure. (Plots of the

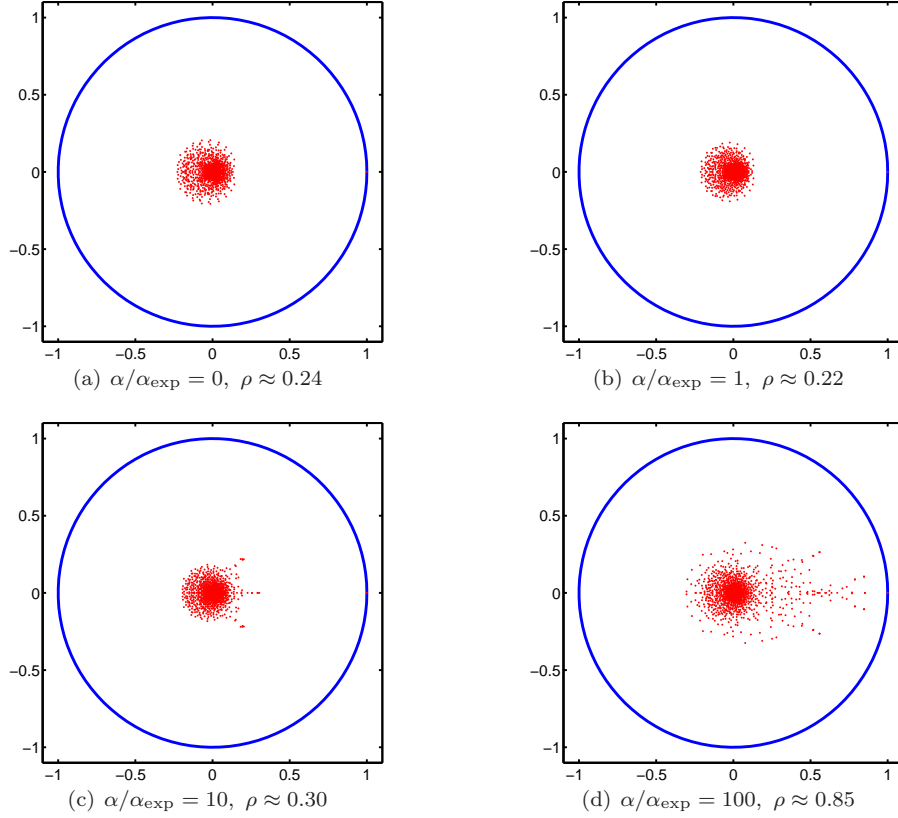


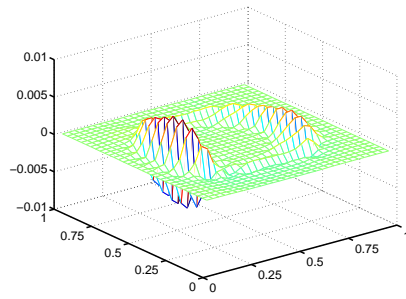
**Fig. 4** Plots of the eigenvalues of the multigrid iteration matrix for four different values of the relative stiffnesses. The value of  $\rho$  is the largest eigenvalue excluding the trivial eigenvalue of 1.

other modes with large eigenvalues have a very similar features and are not shown.) This suggests that the poor performance of the multigrid method results from our failure to smooth the high-frequency modes associated with the elastic structure.

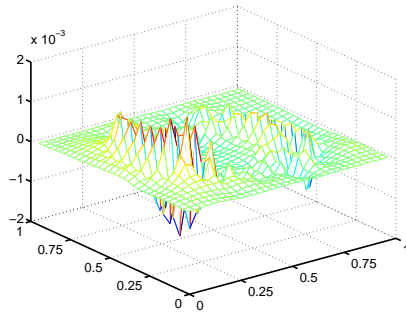
## 6 Big-Box Smoothing

In the previous section, we saw that for large elastic stiffnesses, the multigrid solver with box relaxation required a large number of iterations to converge or failed to converge because it did not smooth high-frequency errors associated with the elasticity of the immersed structure. To understand this phenomenon better, we examine the Eulerian elasticity operator  $S_h A_f S_h^*$ .

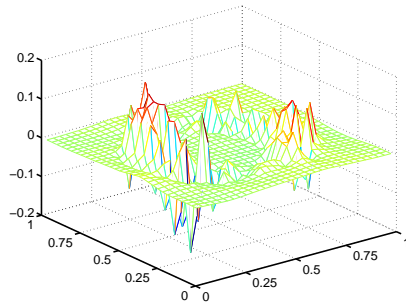
Recall that the operator  $A_f$  represents the second-derivative operator in the fiber direction (i.e., in the circumferential direction in our annulus ex-



(a) horizontal velocity



(b) vertical velocity



(c) pressure

**Fig. 5** Plots of the velocity and pressure corresponding to an eigenvector of the multigrid iteration matrix with eigenvalue 0.8522 for relative stiffness  $\alpha_{\text{exp}}/\alpha$ .

ample), but with no cross-fiber coupling (i.e., in the radial direction). The interpolation operator  $S_h^*$  maps Eulerian data to the Lagrangian mesh, and the spreading operator  $S_h$  maps Lagrangian data to the Eulerian grid. Therefore the operator  $S_h A_f S_h^*$  is in some sense the projection of the fiber-aligned Lagrangian second-derivative operator onto the Eulerian grid. The operator  $(\Delta_h + \alpha S A_f S^*)$  thereby resembles an anisotropic Laplacian operator, in which the degree of the anisotropy increases with the elastic stiffness of the immersed structure.

It is well known that strongly anisotropic problems require smoothers that account for the anisotropy in order to obtain good multigrid performance [35]. When the direction of anisotropy is aligned with the grid, the standard approach is box-line smoothing, in which all the cells in the  $x$ - or  $y$ -directions are collectively updated. For non-grid aligned anisotropy, such methods typically alternate  $x$ -line and  $y$ -line smoothing in two spatial dimensions [35]. The generalization of line smoothing (i.e., plane smoothing) to three spatial dimensions is computationally expensive because it requires repeatedly solving two dimensional problems. Further, these approaches are more expensive than needed for implicit IB methods because the anisotropy is localized to the region covered by the immersed structure.

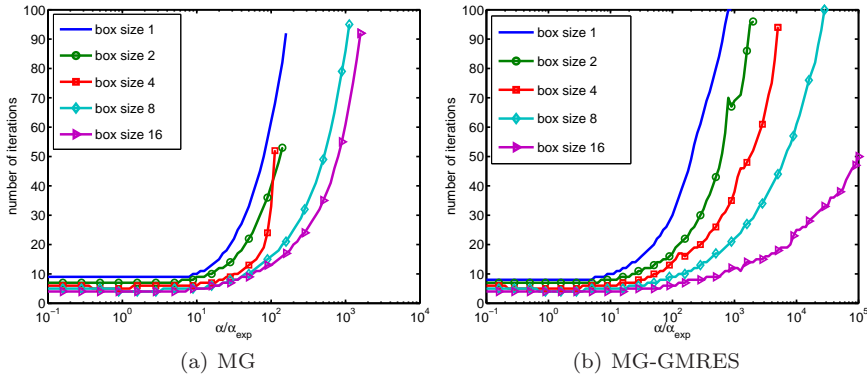
To improve the performance of our multigrid solver and preconditioner, we follow a slightly different block relaxation approach that is still in the spirit of the method introduced by Vanka [37]. Rather than update only the unknowns in a single cell, we instead simultaneously update all unknowns in a rectangular box of size  $n_x \times n_y$ , i.e., with  $n_x$  cells in the  $x$ -direction and  $n_y$  cells in the  $y$ -direction. In the examples in this work, we take  $n_x = n_y$ . We call this approach *big-box smoothing*. As before, the boxes are ordered lexicographically, and one smoothing step involves sweeping over the boxes to update all of the velocities and pressures associated with each  $n_x \times n_y$  box.

Notice that the velocities that lie on the edges of the boxes are updated twice, similar to the original Vanka scheme. It is possible to consider a further generalization of this scheme and consider developing relaxation schemes with additional overlap between boxes. We performed numerical experiments with different overlap sizes, and we did not find a significant advantage in performance to justify the added cost and complexity of including such additional overlap (data not shown).

Our intent in developing such big-box smoothers is to provide a relatively simple approach to smoothing oscillatory components arising from the anisotropic coupling associated with the elasticity of the immersed structure. We note that the  $x$ - and  $y$ -line smoothers can be considered as extreme cases of this scheme with  $n_x = 1$  and  $n_y = N$  (or vice versa). Unlike line smoothers, however, the size of the boxes that we use does not change as the grid is refined. Moreover, our scheme naturally generalizes to three spatial dimensions.

## 6.1 Solver performance

We use the same test problem presented in the previous section. We begin with initial guess of zero for the velocity and pressure, and we record the number of cycles needed to reduce the residual by a factor of  $10^{-6}$  for a range of stiffness. The finest grid is  $32 \times 32$ , and we use V-cycle multigrid with one presmoothing sweep and one postsmoothing sweep ( $\nu_1 = \nu_2 = 1$ ). We perform the test for box sizes  $n_x = n_y = 1, 2, 4, 8, \text{ and } 16$ . The coarsest grid in the V-cycle on which the exact solve is performed is  $N_c \times N_c$  where  $N_c = \max(4, n_x)$ . In later tests the size of the coarsest grid is chosen in the same manor.



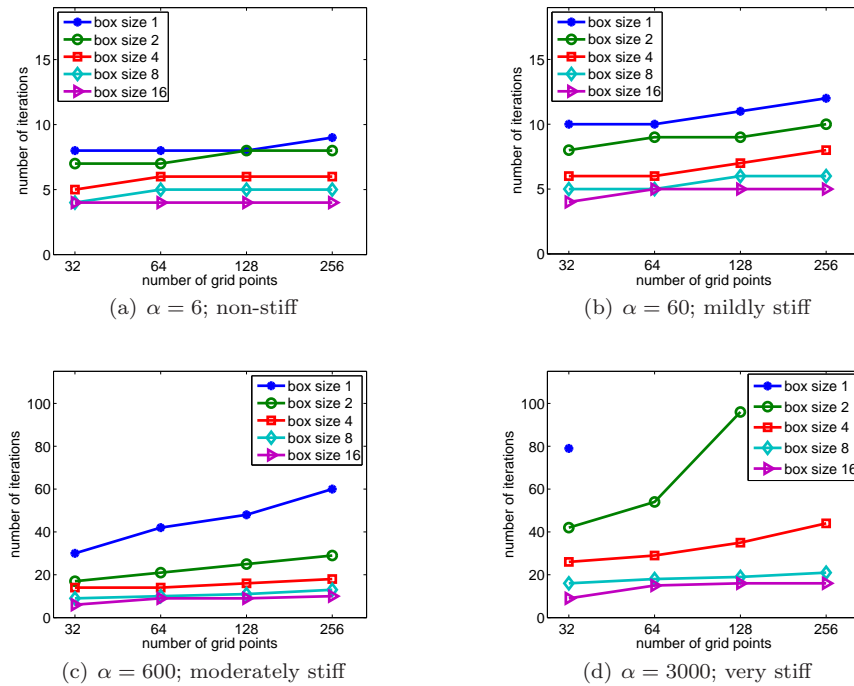
**Fig. 6** Iteration counts for the multigrid and MG-GMRES methods to reduce the residual by a factor of  $10^{-6}$  as a function of the relative stiffness for box smoothers of different sizes.

Figure 6(a) shows iteration counts as a function of stiffness for the stand-alone multigrid solver. The single-box smoothing results from the previous test are also included to facilitate comparison. Interestingly, the method with box sizes 2 and 4 fails at approximately the same stiffnesses as the single-box smoother. Before failure, the iteration counts are smaller with the bigger boxes. Box sizes 8 and 16 show significantly better performance for stiff problems. The iteration count does not start increasing rapidly until a relative stiffness of about 100. The method with box sizes 8 and 16 eventually fails, but at a stiffness that is about an order of magnitude beyond the stiffnesses at which the small-box smoothers fail. Notice that the iteration counts with box size 8 and box size 16 are very similar.

Figure 6(b) shows the iteration counts for MG-GMRES. In general, the larger the box, the lower the iteration count. The difference in iteration counts between the box sizes is particularly pronounced for relatively stiff problems. As the box size is increased, the iteration count rises less steeply as the stiffness increases. For example, for box sizes 2, 4, 8, and 16, the iteration count increases from stiffness 0 to relative stiffness 1000 by a factors of 10, 6, 4, and 3, respectively. These results indicate that for very stiff problems, big-box smoothing in the multigrid algorithm is a very effective preconditioner. Because our tests indicate that MG-GMRES is a much more robust method, from this point on, we present test results only for MG-GMRES.

## 6.2 Effect of grid refinement

So far, all of the tests were performed on an Eulerian grid with fixed grid spacing (specifically,  $N = 32$ ). Here we explore the how grid refinement affects the performance of the MG-GMRES algorithm in the context of the same test problem used previously. We choose four values of the stiffness to explore:  $\alpha = 6$ ,  $\alpha = 60$ ,  $\alpha = 600$ , and  $\alpha = 3000$ . These values of the stiffness roughly



**Fig. 7** Iteration counts of MG-GMRES for different stiffnesses, box sizes, and different grid resolutions. The number of grid points refers to the number of grid cells in each direction on the Eulerian grid.

correspond to relative stiffnesses 1, 10, 100, and 500 on the  $32 \times 32$  grid. We chose these four values to characterize regimes that are non-stiff, mildly stiff, moderately stiff, and very stiff.

Figure 7 shows the number of MG-GMRES iterations needed to reduce the residual by a factor of  $10^{-6}$  for different box sizes and for four different grid resolutions. As before, the maximum number of iterations was set to 100. For the non-stiff and mildly stiff cases (Figure 7(a,b)), the iteration count is essentially independent of the grid size for all box sizes. For the moderately stiff and very stiff cases (Figure 7(c,d)), the iteration count grows as the grid is refined for small boxes, but the iteration count is essentially independent of the grid size for the two largest box sizes (8 and 16). For the very stiff case, the smallest boxes often failed to converge in fewer than 100 iterations; see data for box sizes 1 and 2 in Figure 7(d). These results are consistent with those of the previous section. For mildly stiff problems, small-box smoothers perform well, but for stiff problems, small-box smoothers require a large number of iterations to converge. The difference in performance between big-box smoothers and small-box smoothers is even more striking as the grid is refined.

### 6.3 Cost of smoothing and number of smoothing sweeps

All of the previous results were generated with one presmoothing sweep and one postsmoothing sweep ( $\nu_1 = \nu_2 = 1$ ). Here we explore how the number of smoothing sweeps affects the convergence of the MG-GMRES algorithm for the total number of sweeps per level (i.e.,  $\nu_1 + \nu_2$ ) ranging from 1 to 4. If  $\nu_1 + \nu_2$  is even, then we use an equal number of presmoothing and postsmoothing sweeps, and if  $\nu_1 + \nu_2$  is odd, then we perform one additional presmoothing sweep. We consider box sizes 1, 4, and 8 and relative stiffnesses 10, 100, and 500. As before, these three different stiffnesses characterize the mildly stiff, moderately stiff, and very stiff regimes. The test problem is the same as that used previously. The Eulerian grid spacing is  $h = 2^{-6}$ .

**Table 2** Iteration counts for different relative stiffnesses, box sizes ( $b$ ), and numbers of presmoothing sweeps ( $\nu_1$ ) and postsmoothing sweeps ( $\nu_2$ ). The total work, given in parentheses, is estimated as the number of iterations times ( $\nu_1 + \nu_2 + 1$ ). For each box size and for each stiffness, the entry with the lowest total work is highlighted in bold. (The number of MG-GMRES iterations was capped at 100, and work estimates are not provided for cases requiring more than 100 iterations.)

$b$	$\nu_1$	$\nu_2$	$\alpha/\alpha_{\text{exp}} = 10$	$\alpha/\alpha_{\text{exp}} = 100$	$\alpha/\alpha_{\text{exp}} = 500$
1	1	0	16 (32)	53 (106)	$\geq 100$ (—)
1	1	1	<b>9 (27)</b>	33 (99)	80 (240)
1	2	1	7 (28)	<b>21 (84)</b>	<b>55 (220)</b>
1	2	2	6 (30)	17 (85)	44 (220)
4	1	0	10 (20)	20 (40)	53 (106)
4	1	1	<b>6 (18)</b>	<b>11 (33)</b>	<b>23 (69)</b>
4	2	1	5 (20)	9 (36)	18 (72)
4	2	2	5 (25)	7 (35)	15 (75)
8	1	0	8 (16)	14 (28)	28 (56)
8	1	1	<b>5 (15)</b>	<b>8 (24)</b>	<b>15 (45)</b>
8	2	1	5 (20)	7 (28)	12 (48)
8	2	2	4 (20)	6 (30)	10 (50)

Table 2 shows the number of iterations needed to reduce the residual by a factor of  $10^{-6}$  along with a simple estimate for the amount of computational work required to reach this threshold. The total estimated work to solve the problem is the number of iterations times the work per iteration. We estimate the work per iteration as  $(\nu_1 + \nu_2 + 1)$ ; the “plus one” is included to account for the work per iteration in addition to smoothing. As expected, the iteration count goes down as the number of smoothing sweeps goes up. For each box size and for each stiffness, the entry in Table 2 with the lowest total work is highlighted in bold. For box sizes 4 and 8, one presmoothing sweep and one postsmoothing is always the most efficient choice. For the single-box smoother, an additional smoothing sweep reduces the total work for stiff problems. As our previous results have demonstrated, for very stiff problems, big-box smoothers are more effective.

We remark that our work estimate is based on the total number of smoothing operations and is independent of the size of the box size. This estimate is therefore useful only for comparisons in which the box size is kept fixed. Because each step of the smoother requires solving a linear system on each box, the cost of each smoother sweep increases with box size. However, as our results show, larger boxes also reduce the total number of solver iterations required. It seems likely that there will not generally be a single set of algorithmic options that is most efficient, but instead the optimal choices will depend on the problem, implementation, and possibly the computer architecture.

## 7 Time-Dependent Problem

All of the previous tests focused on solving for the fluid velocity for a prescribed, fixed structure position. In this section, we test the performance of MG-GMRES algorithm in a dynamic IB simulation. We place the same structure used in previous tests in a background shear flow. Unlike the previous tests, here the domain is a rectangle of height 1 and length 2, and the background motion of the fluid is driven by boundary conditions that, in the absence of the elastic structure, would drive the shear flow  $(u, v) = (y, 0)$ . The structure is initially centered at  $\mathbf{x}_c = (0.5, 0.5)$ , and the simulation is run until time  $t = 1$ .

We choose this test because the physical time scale is set by the background flow, not by the stiffness of the structure. This is the type of problem for which implicit-time methods are needed. In Figure 8, we show the structure's position at the end of the simulation. The elastic stiffness affects how much the structure deforms, but the speed of translation is insensitive to the stiffness.

We discretize the Eulerian domain with grid spacing  $h = 2^{-5}$ . For the implicit-time simulations, we fix the time step at  $\Delta t = 1/40$ , and we take 40 time steps. The maximum velocity is about 1, and so the Courant number of these simulations is about 0.8. Although there is no stability constraint on the time step for this problem, we choose to keep the Courant number less than one for reasons of accuracy. Recall that the time-dependent spreading an interpolating operators are lagged in time, and so it is reasonable to require that material points move less than a mesh width per time step.

We use the MG-GMRES method with  $\nu_1 = \nu_2 = 1$  to solve for the fluid velocity to a relative tolerance of  $10^{-6}$  at each time step. Over the course of a simulation, the number of iterations varies slightly from time step to time step. In Figure 9(a), we report the average number of iterations of the solver per time step over the course of the simulation as a function of the relative stiffness for different box sizes. As in the static tests, the iteration counts are fairly constant up to a relative stiffness of 10. Increasing the box size always lowers the iteration count, and the difference in iteration count for different box sizes is particularly striking for very stiff problems.

It is interesting to note that for all box sizes, the iteration count grows sublinearly with the stiffness. For example, at relative stiffness 100, the iter-

ation count increases by a factor of 1.5 (box size 16) to 3 (box size 1) over the iteration count required to solve the Stokes equations alone (i.e., without including the IB elasticity operator). This represents only a small increase in work compared to an explicit-time method, which would require 100 times more time steps to reach the same point in time.

We perform the same simulation using the explicit-time method to compare the performance of the implicit and explicit method. In the explicit-time method, each time step involves solving the Stokes equations for given IB forces. We use the same MG-GMRES method with big-box smoothing for solving the Stokes equations as we used for solving the equations in the implicit-time method. We use time step sizes in the explicit-time simulations that are just below the stability limit. We perform 40 time steps and record the number of MG-GMRES iterations. We extrapolate to estimate the total number of iterations to reach time  $t = 1$ .

We define the efficiency factor as the ratio of the work of the explicit-time method to the work of the implicit-time method needed to complete this simulation. The efficiency factor is the expected speed-up one would gain by using the implicit method in place of the explicit method. To estimate the computational work, we use the number of iterations of the MG-GMRES method. In Figure 9(b), we report the efficiency factor as a function of the relative stiffness for different box sizes. Up to a relative stiffness of about 10, the efficiency factor is similar for all box sizes. As the stiffness increases, larger boxes outperform smaller boxes. These results show that for moderately stiff

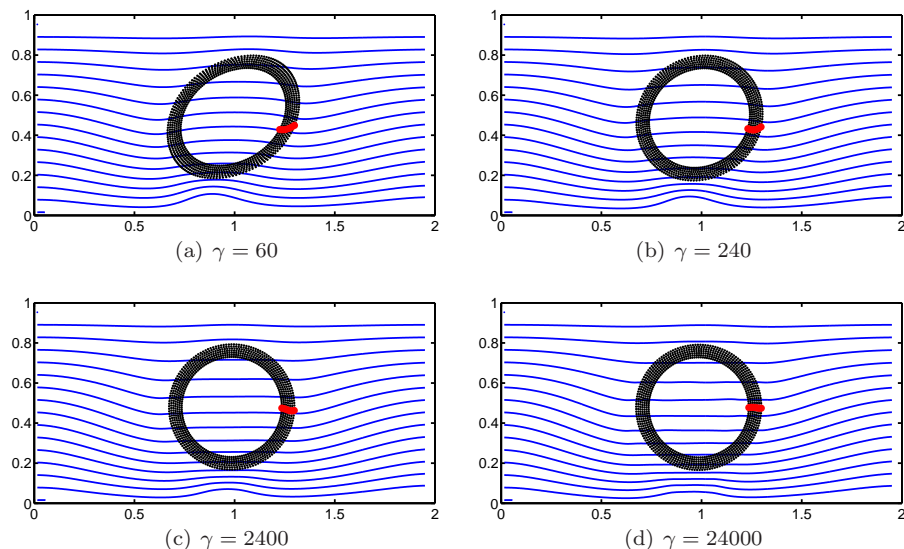


**Fig. 8** Streamlines and structure location at time  $t = 1$  for a range of stiffnesses. The red markers on the structure are used to highlight rotation and internal deformation. At the beginning of the simulation the red markers were aligned horizontally in the  $x$ -direction.

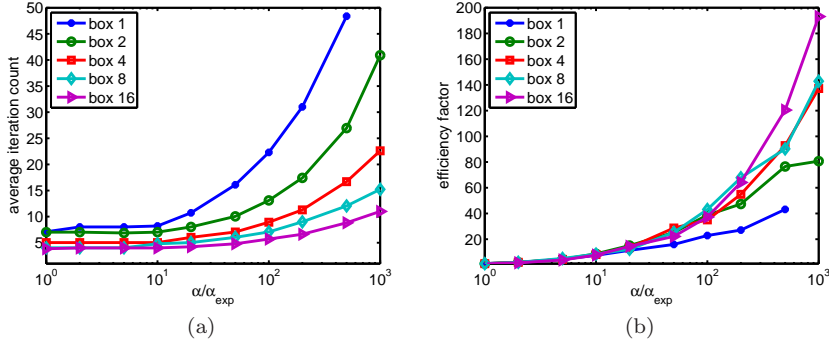


**Fig. 9** (a) Average number of iterations of the MG-GMRES method per time step in the implicit-time simulation. (b) The efficiency factor is the expected speed-up gained by using the implicit method in place of an explicit method.

and very stiff problems, the implicit method with big-box smoothing can be as much as 50–200 times more efficient than an explicit method.

## 8 Discussion

The popularity of the immersed boundary method is driven by its simplicity and robustness. Implementations of the IB method that use explicit-time solution algorithms generally require only solvers for the fluid equations along with routines to compute elastic forces and to transfer data between the Lagrangian mesh and the Eulerian grid. The price of this simplicity is the severe restriction on the largest stable time step permitted by such schemes. One route to overcoming this time step restriction is to develop implicit-time versions of the IB method, but most previously developed implicit-time IB methods use specialized algorithms to achieve substantial speed-ups over explicit-time methods.

The goal of this work is to investigate solution approaches to implicit IB methods that balance efficiency, robustness, and simplicity. A distinguishing feature of our method is that we formulate the problem on the Cartesian grid. This formulation allows the use of standard tools from geometric multigrid to solve the equations. Our algorithm is similar to multigrid methods for the Stokes equations that use coupled smoothing and is relatively straightforward to implement. The major differences between the present algorithm and standard multigrid methods for incompressible flow are the presence of IB elasticity operator  $S_h A_f S_h^*$ , and the use of big-box smoothing. To our knowledge, big-box smoothing has not been proposed previously in the context of incompressible flow problems. Moreover, multigrid-based approaches to developing solvers for implicit IB methods that do not eliminate the Lagrangian degrees of freedom would generally need to resort to approaches such as algebraic multigrid to generate coarse-grid versions of similar operators for cases in which the im-

mersed structure has complex geometry, as is often the case in practice. In our approach, because the relevant elasticity operator is defined on the Cartesian grid, it is straightforward to construct coarse-grid versions of this operator using Galerkin coarsening using the structured-grid restriction and prolongation operators.

Potential limitations of this study are that we restricted our exploration to zero Reynolds number flow and to structures with nonzero thickness with linear constitutive laws. Extensions to nonzero Reynolds numbers are straightforward. In fact, solving the time-independent problem, as we do herein, is *more* challenging than solving the time-dependent problem. The time-dependent problem presents other possible solution methods and preconditioning strategies based on fractional stepping techniques, which do not extend to the time-independent problem. Provided that the nonlinear convection terms are treated explicitly, the system of equations that must be solved at each time step is very similar to (23), with the main difference being that the operator applied to the velocity in the time-dependent problem is  $I - \Delta t \Delta_h - \Delta t^2 \gamma S_h A_f S_h^*$ . The presence of the identity matrix and the appearance of an additional factor of  $\Delta t$  both result in a better conditioned system, and likely will improve the convergence of our method.

In many applications of interest, the elastic structure is modeled as a thin interface of zero thickness. Our method applies equally well to this problem. We choose to use “thick” structures for our numerical tests because the IB method is known to yield poor volume conservation when applied to problems involving thin elastic structures [10]. This unphysical leakage of fluid across the boundary is exacerbated by high elastic stiffness, making it difficult to reach the extreme stiffnesses considered in this work. (Although not shown here, we performed a series of tests with thin boundaries, but the leakage limited our tests to moderate stiffnesses.) Our multigrid solution algorithm performs equally well on thin and thick boundaries, however. The major difference between these two arose upon grid refinement. For a fixed elastic stiffness, thin boundaries become more numerically stiff as the grid is refined. That is, the time step restriction scales like the grid spacing. If the time step is reduced simultaneously with the grid spacing, as is necessary in practice to maintain a fixed Courant number, then the solver performance is essentially grid independent.

In the test problems considered in this paper, the structure inherits the viscosity as the underlying fluid. Immersed boundary methods which include a separate structure viscosity have been developed [7, 16, 32]. A semi-implicit-time discretization which accounts for structure viscosity was proposed and analyzed in [32]. The resulting equations are very similar to those we present in this manuscript, the difference being the form the boundary force operator  $A_f$ , and so our algorithm extends naturally to this type of problem.

Finally, nonlinear constitutive laws could be treated by semi-implicit time stepping schemes that effectively linearize the nonlinear equations. Alternatively, nonlinear time discretizations could be solved via Newton’s method. In either case, it is necessary to solve repeatedly linearized problems of the form considered herein.

A possible criticism of our method is that it requires the use of “big” boxes to achieve a robust solution method. A potential concern with larger boxes is the computational expense of solving the restriction of the full equations to the boxes. We remark that in  $d$  spatial dimensions, each  $n \times n$  box has  $d(n+1)n^{d-1}$  velocity components and  $n^d$  pressure components. For  $d = 2$  and  $n = 4$ , this is a total of 56 degrees of freedom, and if we were to use a dense representation of the box operator, the memory requirements would be approximately 25 KB, which is small enough to fit into high-speed L1 cache on most modern CPUs. In this case, the cost of a direct solver for the box operator will be essentially negligible. For  $d = 3$  and  $n = 4$ , each box has 304 degrees of freedom, and the corresponding dense representation requires approximately 750 KB, which is too large to fit into L1 cache, but which fits comfortably in the L2 or L3 cache available on most systems. Although our tests show that a box size of four does not yield perfect grid-independent convergence rates for extremely stiff systems, it does converge in a reasonable number of iterations and yield good performance compared to an explicit method. We expect that for  $n = 4$ , the local solves will be efficient in a high-quality implementation of the algorithm in either two or three spatial dimensions. Of course, there may be cases in which box sizes greater than four are needed. In these cases, implementations may also be able to exploit the sparsity of the box operators. (Only the “(1,1) block” of the box operator will be relatively dense.) Further, since the restriction of the full operator to the boxes is itself a discrete saddle-point system, for sufficiently large boxes, it may be worthwhile to investigate approximate solution methods.

While our algorithm is simple in spirit, as the foregoing discussion suggests, producing an optimized implementation is not trivial. We estimate that our algorithm will achieve a substantial speed-up over explicit-time methods, but our efficiency estimates are based on iteration counts for a fixed box size, and we did not compare the efficiency across different box sizes. Our initial implementation of the algorithm was not designed with wall-clock efficiency in mind, and fully quantifying the performance of the algorithm requires that we develop an optimized code.

An efficient explicit-time method could exploit that the subsystems associated with the big-box smoother are identical (away from the domain boundaries) and could be pre-factored and stored. Near the immersed boundary the matrix  $S_h A_f S_h^*$  must be reformed at each time step, and the subsystems are all distinct. Reforming  $S_h A_f S_h^*$  does not present a high computational cost because each of these matrices is a sparse matrix with the number of elements proportional the number of immersed boundary points, but this is an additional cost the implicit method that is not reflected in iteration counts alone. However, given the differences in total numbers of iterations required by the implicit and explicit schemes, we believe that it is reasonable to expect to obtain at least order-of-magnitude speed-ups over explicit-time solvers by using optimized implementations of the present implicit-time algorithm. We are in the process of developing optimized versions of our algorithm and including

them in the IBAMR software package [9], and we hope to report results from applications of this code in the future.

## References

1. Boffi, D., Gastaldi, L., Heltai, L., Peskin, C.S.: On the hyper-elastic formulation of the immersed boundary method. *Comput. Methods Appl. Mech. Engrg.* **197**(25-28), 2210 – 2231 (2008)
2. Brandt, A., Dinar, N.: Multi-grid solutions to elliptic flow problems. *Inst. for Computer Applications in Science and Engineering, NASA Langley Research Center, Hampton, Va* (1979)
3. Briggs, W., Henson, V., McCormick, S.: *A Multigrid Tutorial 2nd Edition*. SIAM, Philadelphia (2000)
4. Cenicerros, H.D., Fisher, J.E.: A fast, robust, and non-stiff immersed boundary method. *J. Comput. Phys.* **230**(12), 5133 – 5153 (2011)
5. Cenicerros, H.D., Fisher, J.E., Roma, A.M.: Efficient solutions to robust, semi-implicit discretizations of the immersed boundary method. *J. Comput. Phys.* **228**(19), 7137 – 7158 (2009)
6. Elman, H.C.: Multigrid and krylov subspace methods for the discrete stokes equations. *Internat. J. Numer. Methods Fluids* **22**(8), 755–770 (1996)
7. Fai, T., Griffith, B., Mori, Y., Peskin, C.: Immersed boundary method for variable viscosity and variable density problems using fast constant-coefficient linear solvers I: Numerical method and results. *SIAM J. Sci. Comput.* **35**(5), B1132–B1161 (2013).
8. Gong, Z., Huang, H., Lu, C.: Stability analysis of the immersed boundary method for a two-dimensional membrane with bending rigidity. *Commun. Comput. Phys.* **3**, 704–723 (2008)
9. Griffith, B.E.: IBAMR: An adaptive and distributed-memory parallel implementation of the immersed boundary method. <http://ibamr.googlecode.com>
10. Griffith, B.E.: On the volume conservation of the immersed boundary method. *Commun. Comput. Phys.* **12**, 401–432 (2012)
11. Griffith, B.E., Hornung, R.D., McQueen, D.M., Peskin, C.S.: An adaptive, formally second order accurate version of the immersed boundary method. *J. Comput. Phys.* **223**(1), 10 – 49 (2007)
12. Griffith, B.E., Peskin, C.S.: On the order of accuracy of the immersed boundary method: Higher order convergence rates for sufficiently smooth problems. *J. Comput. Phys.* **208**(1), 75 – 105 (2005)
13. Guy, R.D., Philip, B.: A multigrid method for a model of the implicit immersed boundary equations. *Commun. Comput. Phys.* **12**, 378–400 (2012)
14. Hou, T.Y., Shi, Z.: An efficient semi-implicit immersed boundary method for the navier-stokes equations. *J. Comput. Phys.* **227**(20), 8968 – 8991 (2008)
15. Hou, T.Y., Shi, Z.: Removing the stiffness of elastic force from the immersed boundary method for the 2d stokes equations. *J. Comput. Phys.* **227**(21), 9138 – 9169 (2008). Special Issue Celebrating Tony Leonard’s 70th Birthday
16. Huang, W.X., Sung, H.J.: An immersed boundary method for fluidflexible structure interaction. *Computer Methods in Applied Mechanics and Engineering* **198**(3336), 2650 – 2661 (2009).
17. Le, D., White, J., Peraire, J., Lim, K., Khoo, B.: An implicit immersed boundary method for three-dimensional fluid-membrane interactions. *J. Comput. Phys.* **228**(22), 8427 – 8445 (2009)
18. Lee, L., LeVeque, R.J.: An immersed interface method for incompressible navier–stokes equations. *SIAM J. Sci. Comput.* **25**(3), 832–856 (2003)
19. Linden, J., Lonsdale, G., Steckel, B., Stben, K.: Multigrid for the steady-state incompressible navier-stokes equations: A survey. In: D. Dwoyer, M. Hussaini, R. Voigt (eds.) *11th International Conference on Numerical Methods in Fluid Dynamics, Lecture Notes in Physics*, vol. 323, pp. 57–68. Springer Berlin / Heidelberg (1989)

20. Mayo, A.A., Peskin, C.S.: An implicit numerical method for fluid dynamics problems with immersed elastic boundaries. In: Fluid dynamics in biology (Seattle, WA, 1991), *Contemp. Math.*, vol. 141, pp. 261–277. Amer. Math. Soc., Providence, RI (1993)
21. Mittal, R., Iaccarino, G.: Immersed boundary methods. *Annu. Rev. Fluid Mech.* **37**, 239–261 (2005)
22. Mori, Y., Peskin, C.S.: Implicit second-order immersed boundary methods with boundary mass. *Comput. Methods Appl. Mech. Engrg.* **197**(25-28), 2049 – 2067 (2008). Immersed Boundary Method and Its Extensions
23. Newren, E.P., Fogelson, A.L., Guy, R.D., Kirby, R.M.: Unconditionally stable discretizations of the immersed boundary equations. *J. Comput. Phys.* **222**(2), 702 – 719 (2007)
24. Newren, E.P., Fogelson, A.L., Guy, R.D., Kirby, R.M.: A comparison of implicit solvers for the immersed boundary equations. *Comput. Methods Appl. Mech. Engrg.* **197**(25-28), 2290 – 2304 (2008). Immersed Boundary Method and Its Extensions
25. Niestegge, A., Witsch, K.: Analysis of a multigrid Stokes solver. *Appl. Math. Comput.* **35**(3), 291 – 303 (1990)
26. Oosterlee, C.W., Gaspar, F.J.: Multigrid relaxation methods for systems of saddle point type. *Appl. Numer. Math.* **58**(12), 1933–1950 (2008)
27. Oosterlee, C.W., Washio, T.: An evaluation of parallel multigrid as a solver and a preconditioner for singularly perturbed problems. *SIAM J. Sci. Comput.* **19**, 87–110 (1998)
28. Peskin, C.S.: Numerical analysis of blood flow in the heart. *J. Comput. Phys.* **25**(3), 220 – 252 (1977)
29. Peskin, C.S.: The immersed boundary method. *Acta Numer.* **11**(-1), 479–517 (2002)
30. Saad, Y., Schultz, M.H.: Gmres: A generalized minimal residual algorithm for solving nonsymmetric linear systems. *SIAM J. Sci. Stat. Comput.* **7**(3), 856–869 (1986)
31. Stockie, J.M., Wetton, B.R.: Analysis of stiffness in the immersed boundary method and implications for time-stepping schemes. *J. Comput. Phys.* **154**(1), 41 – 64 (1999)
32. Strychalski, W., Guy, R.D.: Viscoelastic immersed boundary methods for zero Reynolds number flow. *Commun. Comput. Phys.* **12**, 462–478 (2012)
33. Sussman, M., Almgren, A.S., Bell, J.B., Colella, P., Howell, L.H., Welcome, M.L.: An adaptive level set approach for incompressible two-phase flows. *J. Comput. Phys.* **148**(1), 81 – 124 (1999)
34. Tatebe, O.: The multigrid preconditioned conjugate gradient method. In: Proceedings of the Sixth Copper Mountain Conference on Multigrid Methods, pp. 621–634 (1993)
35. Trottenberg, U., Oosterlee, C.W., Schüller, A.: Multigrid. Academic Press, London (2000)
36. Tu, C., Peskin, C.S.: Stability and instability in the computation of flows with moving immersed boundaries: A comparison of three methods. *SIAM J. Sci. Stat. Comput.* **13**(6), 1361–1376 (1992)
37. Vanka, S.P.: Block-implicit multigrid solution of Navier-Stokes equations in primitive variables. *J. Comput. Phys.* **65**(1), 138 (1986)
38. Wittum, G.: On the convergence of multi-grid methods with transforming smoothers. *Numer. Math.* **57**(1), 15 (1990)
39. Wright, G.B., Guy, R.D., Fogelson, A.L.: An efficient and robust method for simulating two-phase gel dynamics. *SIAM J. Sci. Comput.* **30**, 2535–2565 (2008)